

Folding model analysis of elastic and inelastic proton scattering on Sulfur isotopes

Dao T. Khoa^{a *}, Elias Khan^b, Gianluca Colò^c and Nguyen Van Giai^b

^aInstitute for Nuclear Science & Technique, VAEC, P.O. Box 5T-160, Nghia Do, Hanoi, Vietnam.

^bInstitut de Physique Nucléaire, IN2P3-CNRS, 91406 Orsay Cedex, France.

^cDipartimento di Fisica and INFN, Università degli Studi, Via Celoria 16, 20133 Milano, Italy.

The folding formalism for the nucleon-nucleus optical potential and inelastic form factor is applied to study elastic and inelastic proton scattering on $^{30-40}\text{S}$ isotopes. A recently developed realistic density dependent M3Y interaction, well tested in the folding analysis of nucleus-nucleus elastic and inelastic scattering, is used as effective NN interaction. The nuclear ground state and transition densities (for the 2^+ excitations in Sulfur isotopes) are obtained in the Hartree-Fock-BCS and QRPA approaches, respectively. The best fit ratios of transition moments $M_{2^+}^n/M_{2^+}^p$ for the lowest 2^+ states in Sulfur isotopes are compared to those obtained earlier in the DWBA analysis of the same data using the same structure model and inelastic form factors obtained with the JLM effective interaction. Our folding + DWBA analysis has shown quite a strong isovector mixing in the elastic and inelastic scattering channels for the neutron rich $^{38,40}\text{S}$ nuclei. In particular, the relative strength of the isovector part of the transition potential required by the inelastic $p+^{38}\text{S}$ data is significantly stronger than that obtained with the corresponding QRPA transition density.

Keywords: (p,p') reaction, folding model, QRPA transition densities, DWBA analysis

PACS numbers: 24.10.Eq, 24.10.Ht, 24.50.+g, 25.40.Cm, 25.40.Ep, 21.60.Jz

Accepted for publication in Nuclear Physics A

1. INTRODUCTION

The folding model has been used for years to calculate the nucleon-nucleus optical potential (see, e.g., Refs. [1–5]) and inelastic form factors (see, e.g., Refs. [6,7]). It can be seen from the basic folding formulas that this model generates the first-order term of the microscopic optical potential that is derived from Feshbach's theory of nuclear reactions [8]. The success of this approach in describing the observed nucleon-nucleus elastic

*Corresponding author, E-mail: khoa@mail.vaec.gov.vn

scattering data for many targets suggests that the first-order term of the microscopic optical potential is indeed the dominant part of the nucleon optical potential. In the same way, the inelastic (folded) form factor is also the most important input for the analysis of inelastic scattering data within the distorted wave Born approximation (DWBA) or coupled-channel approaches.

The basic inputs for a single-folding calculation of the nucleon-nucleus potential are the nuclear densities of the target and the effective nucleon-nucleon (NN) interaction. If one has a well tested, realistic effective NN interaction, the folding model is a very useful approach to check the target nuclear densities. A popular choice for the effective NN interaction has been one of the M3Y interactions which were designed to reproduce the G-matrix elements of the Reid [9] and Paris [10] NN potentials in an oscillator basis. Although these density *-independent* M3Y interactions were originally developed for use in the DWBA analysis of (p,p') reaction, they have been used much more often in the double-folding calculation of the heavy-ion interaction potential at low and medium energies [11].

Intensive studies of the refractive nucleus-nucleus scattering during the last decade has shown that the simple M3Y-type interaction failed to give a good description of the data, and this has motivated the inclusion into the original M3Y interactions of an explicit density dependence [12–15], to account for the reduction in the (attractive) strength of the effective NN interaction that occurs as the density of the nuclear medium increases [16]. With parameter values chosen to reproduce the observed nuclear matter saturation density and binding energy within the Hartree-Fock (HF) approach, the new density *-dependent* M3Y interactions have been carefully tested in the folding analysis of the refractive nucleus-nucleus elastic scattering [12–15]. In the same HF scheme, parameters of the density dependence of the M3Y interaction are directly associated with the nuclear incompressibility K , and it has been shown that K values ranging from 240 to 270 MeV are the most appropriate for the cold nuclear matter [15] (these values are rather consistent with what can be extracted from the calculations of the isoscalar giant monopole resonance within the relativistic mean field framework; if non-relativistic Skyrme or Gogny forces are employed, slightly lower K values are obtained [17]). The isospin dependence of this interaction was also tested in a HF study of the asymmetric nuclear matter and in the calculation of the heavy-ion potential between nuclei with non-zero isospins [18]. It is therefore of interest to use the new interaction in the folding calculation of the proton-nucleus potential for the analysis of the elastic and inelastic scattering of exotic nuclei on proton target.

In the present work, we adapt the most recent version of the double-folding model [19] for the nucleus-nucleus potential to a single-folding formalism for the elastic and inelastic nucleon-nucleus potentials, using the density- and isospin dependent M3Y interaction. By using the nucleon-nucleus elastic and transition potentials folded with the nuclear densities from a self-consistent microscopic model [20], we have performed a detailed folding analysis of the recent elastic and inelastic $^{30,32}\text{S}+p$ scattering data measured at $E_{\text{lab}} = 53A$ MeV [21] in GANIL, as well as $^{34,36,38,40}\text{S}+p$ data [22–25] measured earlier at $E_{\text{lab}} = 30, 28, 39$ and $30 A$ MeV, respectively. The contributions from isoscalar and isovector parts of the proton-nucleus optical potential and inelastic form factors were treated explicitly in each case to study the isovector mixing effect in the proton-nucleus scattering as one goes along the isotopic chain, from the proton rich ^{30}S to the neutron

rich (short lived) $^{38,40}\text{S}$ isotopes.

2. THE FOLDING MODEL

2.1. General formalism

In the folding model, the proton-nucleus potential V is evaluated as a Hartree-Fock-type potential

$$V_i = \sum_{j \in A} [\langle ij | v_D | ij \rangle + \langle ij | v_{EX} | ji \rangle], \quad (1)$$

where v_D and v_{EX} are the direct and exchange parts of the effective NN interaction between the incident proton i and nucleon j in the target A (in the case of A scattering on proton, A is still treated in our formalism as ‘target’ as given by the inverse kinematics). The antisymmetrization of the system is done by taking into account the knock-on exchange effects (the interchange of nucleons i and j). Due to the antisymmetrization, the potential is, in general, nonlocal in coordinate space. An accurate local approximation is usually obtained by treating the relative motion locally as a plane wave [1,2], and one can reduce the energy-dependent (central) proton-nucleus potential (1) to the following local form

$$V(E, \mathbf{R}) = \int [\rho(\mathbf{r})v_D(\rho, E, s) + \rho(\mathbf{R}, \mathbf{r})v_{EX}(\rho, E, s)j_0(k(E, R)s)] d^3r, \quad (2)$$

where $\mathbf{s} = \mathbf{r} - \mathbf{R}$, \mathbf{R} is the vector joining the center-of-mass of the target and the incident proton, $\rho(\mathbf{r}, \mathbf{r}')$ is the nonlocal (one-body) density matrix (DM) for the target nucleus with $\rho(\mathbf{r}) \equiv \rho(\mathbf{r}, \mathbf{r})$ and $\mathbf{k}(E, R)$ is the local momentum of relative motion determined as

$$k^2(E, R) = \frac{2\mu}{\hbar^2} [E_{\text{c.m.}} - V(E, R) - V_C(R)]. \quad (3)$$

Here, μ is the nucleon reduced mass, $V(E, R)$ and $V_C(R)$ are, respectively, the total nuclear and Coulomb potentials evaluated in the entrance (elastic) channel. The calculation of the *localized* exchange part of the nucleon-nucleus potential [second term in Eq. (2)] still contains a self-consistency problem and involves an explicit integration over the nonlocal nuclear DM. Normally, the density $\rho(\mathbf{r})$ is taken either from a nuclear structure model or directly from electron scattering data. Therefore, the calculation of the exchange potential in Eq. (2) is usually done by using a realistic approximation for the nonlocal DM [1,26]

$$\rho(\mathbf{R}, \mathbf{R} + \mathbf{s}) \simeq \rho\left(\mathbf{R} + \frac{\mathbf{s}}{2}, \hat{j}_1\left(k_F(|\mathbf{R} + \frac{\mathbf{s}}{2}|)s\right)\right),$$

where $\hat{j}_1(x) = 3j_1(x)/x = 3(\sin x - x \cos x)/x^3$. (4)

To accelerate the convergence of the DM expansion, Campi and Bouyssy [26] have suggested to choose the local Fermi momentum $k_F(r)$ in the following form

$$k_F(r) = \left\{ \frac{5}{3\rho(r)} \left[\tau(r) - \frac{1}{4} \nabla^2 \rho(r) \right] \right\}^{1/2}. \quad (5)$$

Assuming this prescription, we choose further the extended Thomas-Fermi approximation [27,28] for the kinetic energy density $\tau(r)$ in the evaluation of the local Fermi momentum

$k_F(r)$. Note that the local approximations made in our approach are essentially the same as those adopted earlier in the folding calculations of nucleon-nucleus optical potential [1–4] and inelastic form factor [6,7].

In this connection, it should be noted that there exists a more sophisticated version of the single-folding model [5] where the nonlocal exchange potential is treated exactly in the Schrödinger equation for the scattering wave function. In this approach one calculates the nonlocal nucleon-nucleus potential using the explicit expression for each single-particle wave function $|j\rangle$ taken, e.g., from the shell model. Therefore, this rigorous approach cannot be used in a general case, when the target wave function is simply represented by a local density distribution $\rho(\mathbf{r})$.

2.2. Explicit treatment of the isospin dependence

Exotic nuclei usually have non-zero isospin and it is necessary to make explicit the isospin degrees of freedom. The spin-isospin decomposition of the (central) NN interaction is

$$\begin{aligned} v_{D(EX)}(\rho, E, s) &= v_{00}^{D(EX)}(\rho, E, s) + v_{10}^{D(EX)}(\rho, E, s)(\boldsymbol{\sigma}\cdot\boldsymbol{\sigma}') \\ &+ v_{01}^{D(EX)}(\rho, E, s)(\boldsymbol{\tau}\cdot\boldsymbol{\tau}') + v_{11}^{D(EX)}(\rho, E, s)(\boldsymbol{\sigma}\cdot\boldsymbol{\sigma}')(\boldsymbol{\tau}\cdot\boldsymbol{\tau}'). \end{aligned} \quad (6)$$

The contribution from the spin dependent terms (v_{10} and v_{11}) in Eq. (6) to the central nucleon-nucleus potential (2) is exactly zero for a spin-saturated target. Even for an odd nucleus, this contribution is at most of A^{-1} effect [29] and is usually neglected in the folding calculation of the central nucleon-nucleus potential.

By writing the nuclear densities in Eq. (2) explicitly in terms of the proton (ρ_p) and neutron (ρ_n) densities, one can represent the proton-nucleus potential (2) in terms of isoscalar (V^{IS}) and isovector (V^{IV}) parts

$$V(E, \mathbf{R}) = V^{IS}(E, \mathbf{R}) + V^{IV}(E, \mathbf{R}). \quad (7)$$

Each term in Eq. (7) has contributions from both the direct and exchange potentials

$$\begin{aligned} V^{IS}(E, \mathbf{R}) &= \int \{[\rho_p(\mathbf{r}) + \rho_n(\mathbf{r})]v_{00}^D(\rho, E, s) \\ &+ [\rho_p(\mathbf{R}, \mathbf{r}) + \rho_n(\mathbf{R}, \mathbf{r})]v_{00}^{EX}(\rho, E, s)j_0(k(E, R)s)\}d^3r. \end{aligned} \quad (8)$$

$$\begin{aligned} V^{IV}(E, \mathbf{R}) &= \int \{[\rho_p(\mathbf{r}) - \rho_n(\mathbf{r})]v_{01}^D(\rho, E, s) \\ &+ [\rho_p(\mathbf{R}, \mathbf{r}) - \rho_n(\mathbf{R}, \mathbf{r})]v_{01}^{EX}(\rho, E, s)j_0(k(E, R)s)\}d^3r. \end{aligned} \quad (9)$$

One can see that the V^{IV} term (microscopic form of the symmetry or Lane potential) is entirely determined by the difference between the proton and neutron densities.

By using the local approximation (4) for the nonlocal proton and neutron ($\tau = p, n$) density matrices

$$\begin{aligned} \rho_\tau(\mathbf{R}, \mathbf{R} + \mathbf{s}) &\simeq \rho_\tau(\mathbf{R} + \frac{\mathbf{s}}{2})\hat{j}_1\left(k_F^\tau(|\mathbf{R} + \frac{\mathbf{s}}{2}|)s\right) \equiv f_\tau(\mathbf{R} + \frac{\mathbf{s}}{2}), \\ \text{where } k_F^\tau(r) &= \left\{ \left[3\pi^2\rho_\tau(r)\right]^{2/3} + \frac{5C_S[\nabla\rho_\tau(r)]^2}{3\rho_\tau^2(r)} + \frac{5\nabla^2\rho_\tau(r)}{36\rho_\tau(r)} \right\}^{1/2}, \end{aligned} \quad (10)$$

the proton-nucleus potential (8)–(9) can be obtained as

$$V^{IS(IV)}(E, \mathbf{R}) = \int [\rho_p(\mathbf{R} + \mathbf{s}) \pm \rho_n(\mathbf{R} + \mathbf{s})] v_{00(01)}^D(\rho, E, s) d^3s \\ + \int \left[f_p(\mathbf{R} + \frac{\mathbf{s}}{2}) \pm f_n(\mathbf{R} + \frac{\mathbf{s}}{2}) \right] v_{00(01)}^{EX}(\rho, E, s) j_0(k(E, R)s) d^3s. \quad (11)$$

In Eq. (10), C_S is the strength of the so-called Weizsäcker term representing the surface contribution to the kinetic energy density. We have adopted the commonly accepted value $C_S=1/36$ [27] which ensures a fast convergence of the density matrix expansion. The local Fermi momentum $k_F^r(r)$ is evaluated using the ground state densities only. The local approximation (10) was shown in a recent folding analysis [28] to be at the level of 1% accuracy.

2.3. Effective density dependent NN interaction

The recently parameterized CDM3Y6 interaction [15], based on the G-matrix elements of the Paris NN potential [10], is used in the present folding calculation. The energy- and density dependences are factorized out as

$$v_{00(01)}^{D(EX)}(E, \rho, s) = g(E)F(\rho)v_{00(01)}^{D(EX)}(s). \quad (12)$$

The explicit density dependence was introduced in Ref. [15]

$$F(\rho) = C[1 + \alpha \exp(-\beta\rho) - \gamma\rho], \quad (13)$$

with parameters adjusted to reproduce saturation properties of nuclear matter and to yield a nuclear incompressibility $K = 252$ MeV in the HF approximation [12,15]

$$C = 0.2658, \quad \alpha = 3.8033, \quad \beta = 1.4099 \text{ fm}^3, \quad \gamma = 4.0 \text{ fm}^3. \quad (14)$$

The ‘intrinsic’ energy dependence of the interaction (to be expected if one regards the effective NN interaction as representing a reaction- or G-matrix of the Brueckner type [30]) is contained in the factor $g(E) \approx 1 - 0.0026\varepsilon$, where ε is the bombarding energy per nucleon (in MeV). The radial strengths of the isoscalar and isovector components of the central M3Y-Paris interaction [10] can be obtained [18] in terms of three Yukawas

$$v_{00(01)}^{D(EX)}(s) = \sum_{\nu=1}^3 Y_{00(01)}^{D(EX)}(\nu) \frac{\exp(-R_\nu s)}{R_\nu s}, \quad (15)$$

where the explicit Yukawa strengths are tabulated in Table 1.

In nucleon-nucleus scattering the most important interaction induced by the nucleon spin is the spin-orbit coupling which is present in both elastic and inelastic channels. The spin-orbit potential arises naturally in the folding model if the effective NN interaction itself has a two-body spin-orbit term

$$v_{LS}(s)\mathbf{L}\cdot\mathbf{S} \equiv v_{LS}(s) \frac{1}{4}[(\mathbf{r}_i - \mathbf{r}_j) \times (\mathbf{p}_i - \mathbf{p}_j)] \cdot (\boldsymbol{\sigma}_i + \boldsymbol{\sigma}_j) \quad (16)$$

For simplicity, we assume that the spin-orbit part of the CDM3Y6 interaction has the same density- and energy dependences as the central part (12)

$$v_{LS}(E, \rho, s) = g(E)F(\rho)v_{LS}(s). \quad (17)$$

Table 1

Yukawa strengths of the central (15) and spin-orbit (18) components of the M3Y-Paris interaction [10,18].

ν	R_ν (fm ⁻¹)	$Y_{00}^D(\nu)$ (MeV)	$Y_{01}^D(\nu)$ (MeV)	$Y_{00}^{EX}(\nu)$ (MeV)	$Y_{01}^{EX}(\nu)$ (MeV)	$Y_{LS}^{(0)}(\nu)$ (MeV)	$Y_{LS}^{(1)}(\nu)$ (MeV)
1	4.0	11061.625	313.625	-1524.25	-4118.0	-5101.0	-1897.0
2	2.5	-2537.5	223.5	-518.75	1054.75	-337.0	-632.0
3	0.7072	0.0	0.0	-7.8474	2.6157	0.0	0.0

The radial strength of the spin-orbit components (with the total isospin T=0 and T=1) of the M3Y-Paris interaction [10] can also be obtained in terms of Yukawas

$$v_{LS}^{(T)}(s) = \sum_{\nu=1}^3 Y_{LS}^{(T)}(\nu) \frac{\exp(-R_\nu s)}{R_\nu s}, \quad (18)$$

with the explicit Yukawa strengths tabulated in Table 1.

2.4. Multipole decomposition

For a consistent description of the elastic and inelastic scattering by the folding potential we need to take into account explicitly the multipole decomposition of the nuclear density [11,19] that enters the folding calculation (7)-(11)

$$\rho_\tau(\mathbf{r}) = \sum_{\lambda\mu} \langle J_A M_A \lambda \mu | J_{A'} M_{A'} \rangle C_\lambda \rho_\lambda^\tau(r) [i^\lambda Y_{\lambda\mu}(\hat{\mathbf{r}})]^*, \quad \text{where } \tau = p, n; \quad (19)$$

J_A and $J_{A'}$ are the target spins in the ground state and excited state, respectively. Usually, the $\lambda = 0$ term represents the ground state density (monopole excitation is a special case and not considered here) and a single multipole $\lambda \neq 0$ dominates in the transition to an excited state with spin $J_{A'}$. In such a case, the corresponding term in the sum (19) represents the nuclear transition density for the excited state. Following Satchler and Love [11], we have chosen here a normalization such that $C_0 = \sqrt{4\pi}$ and $C_\lambda = 1$ for $\lambda \neq 0$. The neutron and proton transition moments are further determined as

$$M_\lambda^\tau = \int_0^\infty \rho_\lambda^\tau(r) r^{\lambda+2} dr. \quad (20)$$

We adopt the same definition of the reduced matrix element as that by Brink and Satchler [31], and the nuclear transition density is such that the reduced electric transition rate for a 2^λ -pole excitation is obtained from the proton transition moment as $B(E\lambda \uparrow) = e^2 |M_\lambda^p|^2$.

The corresponding multipole decomposition of the folded potential (7) can then be written as

$$V(E, \mathbf{R}) = \sum_{\lambda\mu} \langle J_A M_A \lambda \mu | J_{A'} M_{A'} \rangle C_\lambda [V_\lambda^{IS}(E, R) + V_\lambda^{IV}(E, R)] [i^\lambda Y_{\lambda\mu}(\hat{\mathbf{R}})]^*. \quad (21)$$

The isoscalar and isovector parts of the central folded potential (21) consist of the corresponding direct and exchange components

$$V_\lambda^{IS(IV)}(E, R) = V_D^{IS(IV)}(\lambda, E, R) + V_{EX}^{IS(IV)}(\lambda, E, R). \quad (22)$$

We note that if one writes the multipole expansion of the density (19) explicitly through the proton and neutron deformation parameters β_τ , one would end up with the multipole components of the folded potential that depend upon those β values. Such a version of the folding model will be suitable for the analysis of inelastic proton scattering from *deformed* nuclei, as has been studied earlier by Hamilton and Mackintosh in their density dependent folding model [32].

2.5. Direct potential

Using the folding formulas in momentum space [11] the central direct potential can be calculated simply with the density dependent M3Y interaction (12). For the elastic scattering we have $J_{A'} = J_A$ and $\lambda = 0$, and the density components $\rho_0^\tau(r)$ in Eq. (19) are just the proton and neutron ground state densities. Denoting the total ground state density as $\rho_0(r) \equiv \rho_0^p(r) + \rho_0^n(r)$, the direct part of the central elastic potential (22) can be obtained in the following form

$$V_D^{IS(IV)}(\lambda = 0, E, R) = \frac{g(E)}{2\pi^2} \int_0^\infty A_0^{IS(IV)}(q) v_{00(01)}^D(q) j_0(qR) q^2 dq, \quad (23)$$

where the Fourier transforms of the direct interaction and ground state density profile are

$$\begin{aligned} v_{00(01)}^D(q) &= 4\pi \int_0^\infty v_{00(01)}^D(r) j_0(qr) r^2 dr, \\ A_0^{IS(IV)}(q) &= 4\pi \int_0^\infty [\rho_0^p(r) \pm \rho_0^n(r)] F(\rho_0(r)) j_0(qr) r^2 dr. \end{aligned} \quad (24)$$

In evaluating the inelastic form factor (or transition potential) one needs to include the medium corrections implied by the use of a density dependent NN interaction (see, e.g., Refs. [7,19,33]). In a consistent or ‘*dynamic*’ treatment of the density dependence, the change in the density due to the excitation, $\rho \rightarrow \rho_0 + \Delta\rho$, will also change the effective NN interaction

$$F(\rho) v_{D(EX)}(\rho, s) \rightarrow \left[F(\rho_0) + \Delta\rho \frac{\partial F(\rho_0)}{\partial \rho_0} \right] v_{D(EX)}(s). \quad (25)$$

This prescription happens to be exact for the excitation of a single phonon of a 2^λ -pole harmonic shape vibration [34]. In this case, the direct transition potential (22) for a 2^λ -pole excitation of the target can be written in the following form

$$V_D^{IS(IV)}(\lambda, E, R) = \frac{g(E)}{2\pi^2} \int_0^\infty [A_\lambda^{IS(IV)}(q) + B_\lambda^{IS(IV)}(q)] v_{00(01)}^D(q) j_\lambda(qR) q^2 dq, \quad (26)$$

where the Fourier transforms of the transition density profiles are

$$\begin{aligned} A_\lambda^{IS(IV)}(q) &= 4\pi \int_0^\infty [\rho_\lambda^p(r) \pm \rho_\lambda^n(r)] F(\rho_0(r)) j_\lambda(qr) r^2 dr, \\ \text{and } B_\lambda^{IS(IV)}(q) &= 4\pi \int_0^\infty [\rho_0^p(r) \pm \rho_0^n(r)] \rho_\lambda(r) \frac{\partial F(\rho_0(r))}{\partial \rho_0(r)} j_\lambda(qr) r^2 dr. \end{aligned} \quad (27)$$

Here, the total transition density is denoted as $\rho_\lambda(r) \equiv \rho_\lambda^p(r) + \rho_\lambda^n(r)$. It is easy to see that $B_\lambda^{IS(IV)}(q)$ comes from the ‘*dynamic*’ treatment of the density dependent interaction discussed in Eq. (25).

2.6. Exchange potential

The self-consistent (local) exchange potential has to be calculated by an iterative procedure [19], and the exchange part of the elastic potential (22) can be evaluated as

$$V_{EX}^{IS(IV)}(\lambda = 0, E, R) = 2\pi g(E) \int_0^\infty G_0^{IS(IV)}(R, s) v_{00(01)}^{EX}(s) j_0(k(E, R)s) s^2 ds, \quad (28)$$

$$\text{where } G_0^{IS(IV)}(R, s) = \int_{-1}^1 [f_0^p(y(x), s) \pm f_0^n(y(x), s)] F(\rho_0(y(x))) dx,$$

$$y(x) = \sqrt{R^2 + \frac{s^2}{4} + Rxs} \quad \text{and} \quad f_0^\tau(y, s) = \rho_0^\tau(y) \hat{j}_1(k_F(y)s). \quad (29)$$

After some integral transformation using the expansion formula [35] for spherical harmonics of the mixed argument $Y_{\lambda\mu}(\widehat{\mathbf{R} + \mathbf{s}})$, the exchange transition potential (22) for a 2^λ -pole excitation of the target can be written as

$$\begin{aligned} V_{EX}^{IS(IV)}(\lambda, E, R) &= 2\pi g(E) \int_0^\infty [G_\lambda^{IS(IV)}(R, s) + H_\lambda^{IS(IV)}(R, s)] \\ &\times v_{00(01)}^{EX}(s) j_0(k(E, R)s) s^2 ds, \end{aligned} \quad (30)$$

where the exchange kernels are

$$\begin{aligned} G_\lambda^{IS(IV)}(R, s) &= R^\lambda \int_{-1}^1 [f_\lambda^p(y(x), s) \pm f_\lambda^n(y(x), s)] \frac{F(\rho_0(y(x)))}{[y(x)]^\lambda} dx, \\ H_\lambda^{IS(IV)}(R, s) &= R^\lambda \int_{-1}^1 [f_0^p(y(x), s) \pm f_0^n(y(x), s)] \frac{\rho_\lambda(y(x))}{[y(x)]^\lambda} \left[\frac{\partial F(\rho_0(y(x)))}{\partial \rho_0(y(x))} \right] dx, \end{aligned} \quad (31)$$

with $f_\lambda^\tau(y, s) = \rho_\lambda^\tau(y) \hat{j}_1(k_F(y)s)$. Note that we have implied the same dynamic treatment of the density dependence (25) which leads to the $H_\lambda^{IS(IV)}(R, s)$ kernel.

2.7. Spin-orbit and Coulomb potentials

In the elastic channel, in addition to the central potential $V_0^{IS(IV)}(E, R)$, the nucleon-nucleus optical potential has also the spin-orbit part $V_{LS}(\lambda = 0, E, R)(\mathbf{l} \cdot \boldsymbol{\sigma})$. In many cases, a phenomenological Thomas form for the spin-orbit potential suffices for a good description of the elastic data if the strength is adjusted properly. Within the folding model, the spin-orbit potential can be evaluated microscopically using the two-body spin-orbit NN interaction and the nuclear density of the target. We have chosen the local approximation developed by Brieva and Rook [3] and evaluated $V_{LS}(\lambda = 0, E, R)$ using the spin-orbit component of the CDM3Y6 interaction (17)-(18), with the isospin dependence treated explicitly,

$$V_{LS}(\lambda = 0, E, R) = -\frac{g(E)F(\rho_0(R))}{3} \left[\Phi_p(E, R) \frac{1}{R} \frac{d\rho_0^p(R)}{dR} + \Phi_n(E, R) \frac{1}{R} \frac{d\rho_0^n(R)}{dR} \right], \quad (32)$$

$$\Phi_p(E, R) = \int_0^\infty v_{LS}^{(1)}(s) [1 + \hat{j}_1(k(E, R)s)] s^4 ds,$$

$$\Phi_n(E, R) = \frac{1}{2} \int_0^\infty \{v_{LS}^{(1)}(s) [1 + \hat{j}_1(k(E, R)s)] + v_{LS}^{(0)}(s) [1 - \hat{j}_1(k(E, R)s)]\} s^4 ds. \quad (33)$$

In its general formulation, the spin-orbit interaction also contributes to the inelastic scattering channel and one needs to explicitly calculate the scattering amplitude in the DWBA formalism, using the spherical tensor expansion of the spin-orbit interaction and explicit wave function for each single-particle configuration involved in the excitation [36,38]. Such a method is not applicable if the target excitation is simply represented by a nuclear transition density $\rho_\lambda(r)$. Here, we have adopted the same local approximation [3] as in the elastic case and inserted (19) into the local density expression. In the first-order approximation, the spin-orbit transition potential can be obtained as

$$V_{LS}(\lambda, E, R) = -\frac{g(E)F(\rho_0(R))}{3} \left[\Phi_p(E, R) \frac{1}{R} \frac{d\rho_\lambda^p(R)}{dR} + \Phi_n(E, R) \frac{1}{R} \frac{d\rho_\lambda^n(R)}{dR} \right], \quad (34)$$

where $\Phi_\tau(E, R)$ is determined by the same formula (33). Note that for the natural-parity excitations considered in this work, the central transition potential gives a dominant contribution to the inelastic cross section, and the transition spin-orbit potential (34) has only a minor effect.

The proton-nucleus optical potential or inelastic transition potential, calculated by the folding model, has to be supplemented by a corresponding Coulomb potential. It is straightforward to use the same folding method to evaluate microscopically the proton-nucleus Coulomb potential, using the (target) charge density matrix

$$V_C(E, \mathbf{R}) = \int \frac{e^2}{|\mathbf{r} - \mathbf{R}|} [\rho_{\text{charge}}(\mathbf{r}) - \rho_{\text{charge}}(\mathbf{R}, \mathbf{r}) j_0(k(E, R)|\mathbf{r} - \mathbf{R}|)] d^3r. \quad (35)$$

One can use the same local approximation (10) for the nonlocal proton density matrix and then take into account the finite proton size[11] to obtain the charge distribution $\rho_{\text{charge}}(\mathbf{r})$ for the calculation of the Coulomb potential (35). $V_C(E, \mathbf{R})$ can then be expanded into a multipole series analogous to that of Eq. (21) for the nuclear potential.

In the optical model (OM) analysis of elastic proton-nucleus scattering, the Coulomb potential $V_C(\lambda = 0, E, R)$ is usually represented by the Coulomb potential between a point charge and a uniform charge distribution of radius $R_C = r_C A^{1/3}$. This option for the elastic Coulomb potential can be shown to have about the same strength and shape at the surface as the microscopic potential obtained from Eq. (35). For convenience in referring or comparing with other results, we have chosen this option for the elastic Coulomb potential in our OM calculation.

In the DWBA analysis of inelastic proton-nucleus scattering with a 2^λ -pole excitation of the target, the transition Coulomb potential $V_C(\lambda, E, R)$ has been often taken in a model- and energy independent asymptotic form that can be expressed in terms of the reduced electric transition rate $B(E\lambda)$ (see, e.g., Refs. [19,29]). Since a correct input for the Coulomb form factor is substantial in the analysis of the low-lying electric type excitations, we have used in the present work the microscopic Coulomb form factor given by Eq. (35).

2.8. Complex elastic and inelastic potentials

The original M3Y interaction (15) is real, and the formalism presented above can be used to generate the real parts of the elastic and inelastic nucleon-nucleus potentials only. These must be supplemented by imaginary potentials which account for the absorption

into other channels that are allowed energetically but are not considered explicitly. This absorption contributes imaginary parts to both the diagonal (elastic) and the off-diagonal (inelastic) potentials. It is common to resort to a hybrid approach by using the folding model to generate the real part but to use the standard Woods-Saxon (WS) potential for the imaginary part, and the local nucleon-nucleus optical potential is

$$U_0(E, R) = V_0(E, R) + iW_0(E, R) + V_{LS}(\lambda = 0, E, R)(\mathbf{l} \cdot \boldsymbol{\sigma}), \quad (36)$$

where the real and imaginary parts of the (central) optical potential are given by

$$\begin{aligned} V_0(E, R) &= V_C(R) + N_R[V_D(0, E, R) + V_{EX}(0, E, R)], \\ W_0(E, R) &= -\frac{W_V}{1 + \exp((R - R_W)/a_W)} - \frac{4W_S \exp((r - R_W)/a_W)}{[1 + \exp((r - R_W)/a_W)]^2}. \end{aligned} \quad (37)$$

Here $V_C(R)$ is the Coulomb potential between a point charge and a uniform charge distribution of radius $R_C = r_C A^{1/3}$, $R_W = r_W A^{1/3}$ and the real optical potential $V_{D(EX)}(0, E, R)$ is calculated by using Eqs. (23) and (28). The choice of the parameters for the WS imaginary potential can be made using the available systematics for the nucleon optical potential. The accurate CH89 global systematics [39], based on several thousands data sets for the nucleon-nucleus elastic scattering at energies ranging from 10 to 65 MeV, is used in this work to parameterize the imaginary part of the optical potential. The normalization factor N_R for the real (folded) optical potential is adjusted in each case to fit the elastic data. In the present folding approach, N_R is an approximate way to make small adjustments that may be needed to take into account the higher order contributions to the (real) microscopic optical potential, the so-called ‘dynamic polarization potential’ (DPP) in the Feshbach’s formalism [8]. It is obvious that value of N_R should remain close to unity for this procedure to be reasonable.

We stress that a reaction- or G-matrix calculation for a single nucleon incident on nuclear matter [30] can lead to a complex effective NN interaction (like the JLM effective interaction), where the absorption is associated with the finite mean free path of nucleons in *nuclear matter*. The imaginary part of such an effective NN interaction (obtained in a standard local density approximation) does not account in principle for the important sources of absorption in *finite nuclei* like the excitation of surface modes, nucleon transfer and breakup reactions, etc. These non-elastic processes contribute to the energy dependent, nonlocal and complex DPP that gives rise to the imaginary part of the optical potential [8].

We apply further the same hybrid scheme to the inelastic (transition) potential, and the transition potential for a 2^λ -pole excitation is

$$U_\lambda(E, R) = V_\lambda(E, R) + iW_\lambda(E, R) + V_{LS}(\lambda, E, R)(\mathbf{l} \cdot \boldsymbol{\sigma}), \quad (38)$$

where the real and imaginary parts of the (central) inelastic potential are given by

$$\begin{aligned} V_\lambda(E, R) &= V_C(\lambda, E, R) + V_D(\lambda, E, R) + V_{EX}(\lambda, E, R), \\ W_\lambda(E, R) &= -\delta_\lambda \frac{\partial W_0(E, R)}{\partial R}. \end{aligned} \quad (39)$$

Thus, the real nuclear, Coulomb and spin-orbit transition form factors are calculated by the folding approach, while a conventional approach of the collective vibration model is

used to obtain the imaginary transition form factor. In the present work we have assumed δ_λ equal to the charge deformation length, which is determined from the reduced electric transition rate $B(E\lambda \uparrow)$ [29] as

$$\delta_\lambda = \frac{4\pi\sqrt{B(E\lambda \uparrow)/e^2}}{(\lambda + 2)Z \langle r^{\lambda-1} \rangle_p}, \quad \text{where} \quad \langle r^{\lambda-1} \rangle_p = \frac{\int \rho_0^p(r)r^{\lambda+1}dr}{\int \rho_0^p(r)r^2dr}. \quad (40)$$

The obtained charge deformation lengths for the lowest 2^+ states in Sulfur isotopes are given in Table 2. We note that the real central and spin-orbit inelastic form factors in Eq. (39) were used in the DWBA calculation as given by the folding model, without a normalization factor. In the past, one has often used the same normalization factor N_R for both the elastic and inelastic folded (central) potentials. Such a method is ‘consistent’ if one considers N_R of the real (folded) optical potential as scaling factor of the effective NN interaction for a particular target at the given incident energy. In our case, parameters of the CDM3Y6 interaction have been fine-tuned, in the HF calculation, to reproduce the saturation properties of nuclear matter (with a realistic value of the nuclear incompressibility $K \approx 252$ MeV [15]) and energy dependence of the nucleon-nucleus optical potential [12,37]. Thus, the CDM3Y6 interaction should be suitable for any target (at different energies) and no further scaling of the interaction is expected (because it would affect the established HF results, on which the interaction is based). Therefore, one needs to consider the normalization factor N_R of the real (folded) optical potential in (37) approximately as an effect caused by contribution of the DPP to the (real) microscopic optical potential only. Given the effective NN interaction carefully parameterized, it is reasonable to use the folded inelastic form factor without re-normalization in the (one-channel) DWBA calculation of inelastic scattering if the higher-order contribution from the DPP to the real inelastic folded form factor is weak. We will discuss this aspect again in Sec. 4

All the OM and DWBA analyses of elastic and inelastic proton scattering were made using the code ECIS97 written by J. Raynal [38].

3. THE NUCLEAR DENSITIES

Different kinds of nuclear densities can be used as input of the present folding approach. Actually, Eqs. (19) and (20) refer to a macroscopic description (see, e.g., p.579 of Ref. [29]), and the expression (19) should be interpreted as a generic deformed density of an excited spherical nucleus, in which the $\lambda \neq 0$ multipole terms represent the difference with respect to the ground state density and may be used as transition densities for inelastic transition to natural parity states of multipolarity λ , provided they are properly normalized. On the other hand, the present folding approach can naturally accommodate, within its framework, the microscopic nuclear ground state and transition densities (see also p.657 of Ref. [29]) and we believe it is worth to study the predictive power of the model by using these microscopic nuclear structure inputs. In this section, we briefly describe the structure model used to obtain the nuclear ground state and transition densities, having in mind the application of the model to the neutron rich Sulfur isotopes and giving some details relevant to this case.

We work in the framework of self-consistent calculations based on Hartree-Fock plus Random Phase Approximation (HF+RPA) with the use of Skyrme interactions. This nuclear structure model has been used for a long time to determine the structure properties of the nuclear vibrational states, especially, the giant resonances. Recently it has been extended to include pairing correlations by performing quasi-particle RPA (QRPA) calculations on top of HF+BCS [20,21] (see also Ref. [40]). In the study of nuclei along extended isotopic chains the inclusion of pairing is indeed called for, and its effect is expected to be important in the open shell isotopes, especially in the case of low-lying excitations.

3.1. The nuclear ground state densities

In this work, we perform spherical HF+BCS calculations in coordinate space using the SGII parameterization [44] of the Skyrme interaction. We choose a simple prescription for the pairing interaction by assuming a constant pairing gap given by $\Delta = 12/\sqrt{A}$ MeV [45]. The use of a constant pairing gap produces unrealistic results (states at relatively high energy acquire quite large occupation probabilities) unless a cutoff is set in the single-particle space such that states above this cutoff do not feel any pairing interaction. In the case of the Sulfur isotopes, this cutoff is chosen such as to include all the subshells of the major shell to which the Fermi level belongs. The ground state neutron and proton densities are then obtained as

$$\rho_0^\tau(r) = \sum_{\alpha} v_{\alpha}^2 \varphi_{\alpha}(r), \quad (41)$$

where $\varphi_{\alpha}(r)$ and v_{α} are the radial wave function and BCS amplitude of the quasi-particle state $|\alpha\rangle$, respectively. The summation on α runs over neutrons (protons) for $\tau=n$ ($\tau=p$).

3.2. The nuclear transition densities

We briefly recall the main steps of the QRPA calculations [20]. Based on the HF+BCS quasi-particle basis, the QRPA equations are solved in the configuration space, using the standard matrix form. The residual interaction between quasi-particles is derived from the Skyrme force used in the HF+BCS calculation, without including the pairing contribution. The continuous part of the single quasi-particle spectrum is discretized by diagonalizing the HF+BCS Hamiltonian on a harmonic oscillator basis. The size of the QRPA model space, i.e., the number of two quasi-particle configurations included, is chosen large enough to exhaust the appropriate energy-weighted sum rule. Solving the QRPA equations provides us with the energies ω_{κ} as well as the wave functions of the excited states $|\kappa\rangle$ of a given multipolarity λ . These wave functions are normally given in terms of the well-known amplitudes $X_{\alpha\beta}^{\kappa}$ and $Y_{\alpha\beta}^{\kappa}$, with $\alpha\beta$ denoting the involved two quasi-particle configurations. The nuclear transition to the excited state $|\kappa\rangle$ can be characterized by the corresponding (local) proton or neutron transition densities $\Delta\rho_{\kappa}^{\tau}(\mathbf{r})$ defined as

$$\Delta\rho_{\kappa}^{\tau}(\mathbf{r}) \equiv \langle \kappa | \sum_i \delta(\mathbf{r} - \mathbf{r}_i) | \text{g.s.} \rangle, \quad (42)$$

where the summation on i runs over neutrons (protons) for $\tau=n$ ($\tau=p$).

Table 2

The excitation energy ω , reduced electric transition probability $B(E2 \uparrow)$ and ratio of quadrupole transition moments $M = (M_{2^+}^n/M_{2^+}^p)/(N/Z)$ for the lowest 2^+ states in Sulfur isotopes, as given by QRPA (see Sec. 3). The ‘experimental’ M_{exp} ratio is obtained by scaling the proton part of the QRPA transition density to reproduce the experimental $B(E2)_{\text{exp}}$ value and adjusting the neutron part to the best DWBA fit to the inelastic scattering data. The ‘phenomenological’ M_{Phenom} ratio was obtained in Refs. [21,25] based on standard collective model form factor. The experimental values for ω_{exp} and $B(E2)_{\text{exp}}$ are taken from Refs. [41–43]. The charge deformation lengths δ_2 are determined from the corresponding $B(E2)_{\text{exp}}$ values using Eq. (40).

Nucleus	ω_{QRPA} (MeV)	ω_{exp} (MeV)	$B(E2)_{\text{QRPA}}$ ($e^2\text{fm}^4$)	$B(E2)_{\text{exp}}$ ($e^2\text{fm}^4$)	δ_2 (fm)	M_{QRPA}	M_{exp}	M_{Phenom}
^{30}S	2.79	2.21	327	320 ± 40	1.19	1.05	1.05	0.93 ± 0.20
^{32}S	2.94	2.23	294	300 ± 13	1.14	0.96	0.96	0.95 ± 0.11
^{34}S	2.65	2.13	256	212 ± 12	0.95	0.94	1.04	0.91 ± 0.11
^{36}S	3.46	3.29	241	96 ± 26	0.63	0.64	0.90	1.13 ± 0.27
^{38}S	2.19	1.30	325	235 ± 30	0.98	0.98	1.44	1.50 ± 0.30
^{40}S	1.54	0.89	431	334 ± 36	1.17	1.03	1.17	1.25 ± 0.25

It is evident from this definition (see also p.657 of Ref. [29]) that these are the appropriate quantities to be folded with the NN interaction to obtain the inelastic proton-nucleus form factors as described in Sec. 2. The explicit radial form of the QRPA transition density, for the transition to an excited state $|\kappa\rangle$ of the multipolarity λ , is

$$\Delta\rho_{\kappa}^{\tau}(r) \equiv \rho_{\lambda}^{\tau}(r) = \sum_{\alpha \geq \beta} \varphi_{\alpha}(r)\varphi_{\beta}^{*}(r) \langle \beta || Y_{\lambda} || \alpha \rangle > \{X_{\alpha\beta}^{\kappa} - Y_{\alpha\beta}^{\kappa}\} \{u_{\alpha}v_{\beta} + (-1)^{\lambda}v_{\alpha}u_{\beta}\}. \quad (43)$$

The HF+BCS ground state (41) and QRPA transition densities (43) of the considered Sulfur isotopes are those obtained recently by the Orsay group [21] (see, e.g., the radial shape of these densities in Figs. 10 and 11 of Ref. [21]). In particular, the QRPA charge ground-state and transition densities for $^{32,34}\text{S}$ have been shown to reproduce reasonably well the experimental charge densities of these isotopes (measured directly by electron scattering). It should be noted that these transition densities have been previously used to obtain the inelastic S+p form factors using the JLM effective interaction [21]. Therefore, the comparison of the results obtained for the Sulfur isotopic chain will lend crucial information on the validity of reaction models (see further discussion in Sec. 4).

Among the integral properties of the QRPA transition densities, the most important ones are the reduced transition probabilities $B(E\lambda \uparrow)$ and the ratio of the transition moments $M_{\lambda}^n/M_{\lambda}^p$, as determined by Eq. (20). In a simple collective model [45,46], the oscillation of the homogeneous neutron-proton fluid is so-called purely isoscalar if $M_{\lambda}^n/M_{\lambda}^p = N/Z$. Consequently, a significant deviation of $M_{\lambda}^n/M_{\lambda}^p$ from N/Z would indicate the degree of what we call the *isovector mixing* in the considered quadrupole excitations. We will discuss this as well as other structure effects in more details in the next Section.

4. RESULTS AND DISCUSSION

4.1. Elastic scattering

For any nucleon-nucleus system, the accurate measurement of the elastic scattering provides essential information for the determination of the nucleon-nucleus optical potential, which is further used to generate the distorted waves for the calculation of inelastic scattering amplitude in the DWBA formalism. The considered elastic $^{30-40}\text{S}+\text{p}$ scattering data at different energies have been analyzed in the present work with the optical potential obtained from Eqs. (36) and (37). The real optical potential was obtained using the CDM3Y6 interaction and the ground-state densities given by the HF+BCS calculation, while the WS imaginary potential was parameterized using the CH89 global systematics [39]. The best-fit optical model parameters are given in Table 3. From the results plotted in upper parts of Figs. 1-4 one can see that our folding potential reproduces the elastic data quite well. Although the CH89 parameters are mainly based on the nucleon-nucleus elastic data for medium-mass targets, they seem to be able to provide a reasonable estimate for the Sulfur isotopes as well. In the $^{30}\text{S}+\text{p}$ and $^{40}\text{S}+\text{p}$ cases, the CH89 parameters of the WS imaginary part of the optical potential are very appropriate and only the renormalization factor N_R of the real folded potential was slightly adjusted by the OM search to fit the elastic data. For the $^{32-38}\text{S}$ isotopes, the strengths W_V, W_S were also adjusted by the OM fit and the calculated elastic cross sections agree very well with the measurement. The obtained OM parameters (Table 3) have been used further in all the

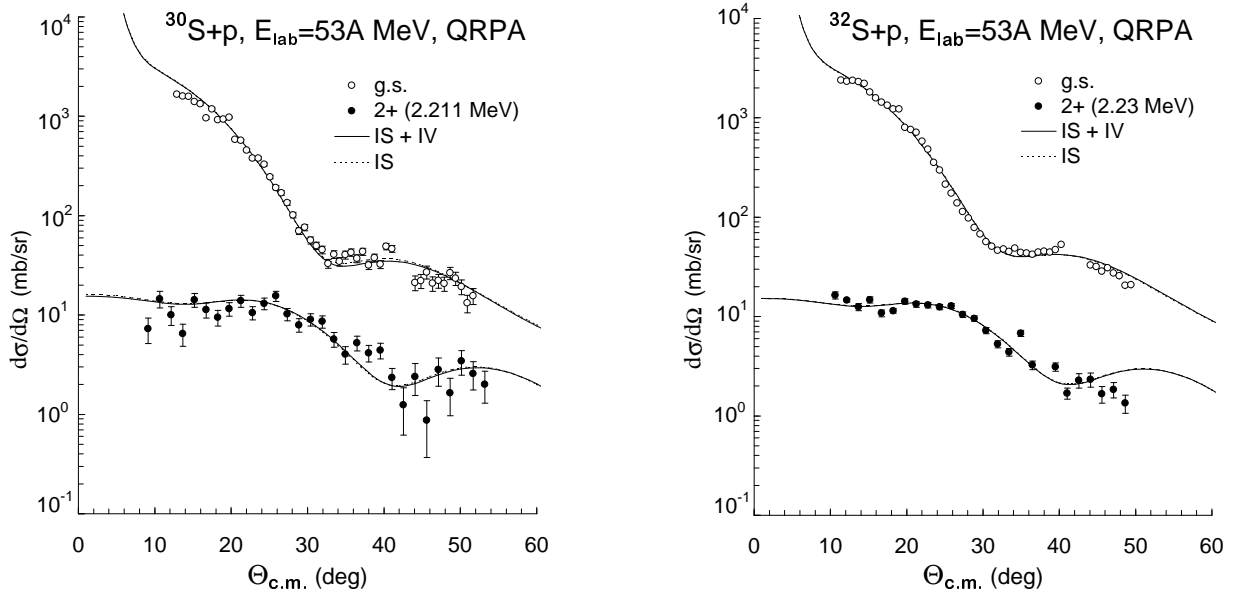


Figure 1. Elastic and inelastic $^{30,32}\text{S}+\text{p}$ scattering data at $E/A = 53$ MeV [21] in comparison with the DWBA cross sections given by the elastic and inelastic potentials folded with the HF+BCS ground-state and QRPA transition densities, respectively. The cross sections given by the isoscalar potentials alone are plotted as dotted curves.

We note that the recently measured elastic $^{30,32}\text{S}+\text{p}$ data at $E/A = 53$ MeV [21]

are quite accurate and have more data points compared to other cases. To show the reliability of the semi-microscopic optical potential obtained in the present approach, we have further plotted in Fig. 2 the elastic $^{30,32}\text{S}+p$ data and the calculated cross section in ratio to Rutherford cross section (because the actual quality of the OM fit then becomes more transparent). One can see that the oscillating structure of the elastic cross section becomes more pronounced if plotted as ratio to Rutherford, and our OM results give indeed a ver

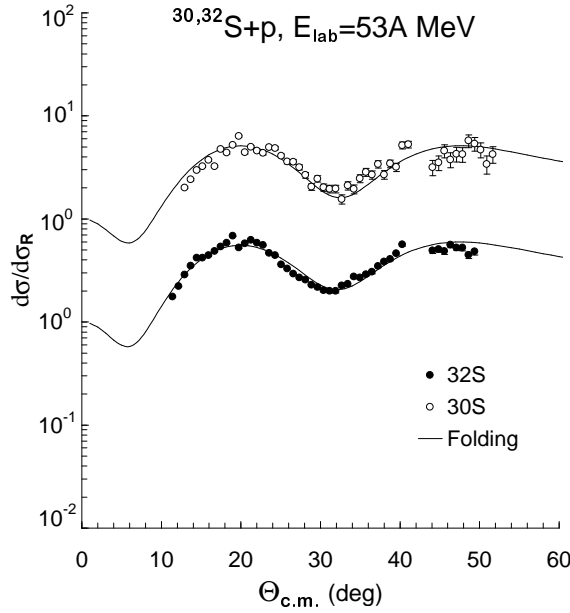


Figure 2. Elastic $^{30,32}\text{S}+p$ scattering data at $E/A = 53$ MeV [21] and results of the present OM calculation plotted in ratio to corresponding Rutherford cross section.

In recent years, various experimental studies of reaction cross sections have been done to probe the nuclear sizes, especially the existence of halo or neutron skin in unstable nuclei [47]. It is, therefore, of interest to present the calculated total reaction cross sections σ_R for the considered cases (see Table 3). From the relative difference $\Delta\sigma_R$ between the total reaction cross section given by our folding analysis and that given by the mass- and energy dependent systematics for stable isotopes (see Eq. (1) in Ref. [48]), one finds that our results agree with the systematics within about 10%. $\Delta\sigma_R$ is only 5% for ^{32}S (a stable, $N = Z$ isotope), and we do not see any enhancement in σ_R for the proton-rich ^{30}S isotope that might indicate a proton halo in this nucleus. To provide crucial data on this point, measurements at large center-of-mass angles are called for. Note that the total reaction cross section is mainly determined by the imaginary part of the optical potential, and the large angle data, if available, would reduce the uncertainty in the absorption strength and σ_R values can be extracted more precisely. Among the Sulfur isotopes under study $\Delta\sigma_R$ is largest for ^{40}S (about 18%) which is clearly due to the neutron skin in this neutron-rich (unstable) isotope. The neutron (proton) r.m.s. radii calculated within HF+BCS for this

Table 3

OM parameters [see Eqs. (36) and (37)] used in the folding analysis of the elastic proton scattering on Sulfur isotopes. The real optical potentials were folded with the CDM3Y6 interaction and ground-state densities given by the HF+BCS calculation. Starting parameters of the WS imaginary optical potential and Coulomb radius were taken from the global systematics CH89 [39]. Parameters which were fixed during the OM search are given in boldface.

Target	E/A (MeV)	N_R	W_V (MeV)	W_S (MeV)	r_W (fm)	a_W (fm)	r_C (fm)	σ_R (mb)	$\Delta\sigma_R$ (%)
^{30}S	53	0.940	5.347	3.723	1.195	0.690	1.275	669.4	12
^{32}S	53	0.901	4.037	3.480	1.198	0.690	1.275	643.3	5
^{34}S	30	0.930	3.949	6.315	1.200	0.690	1.274	937.5	12
^{36}S	28	0.947	1.074	6.968	1.203	0.690	1.273	945.7	11
^{38}S	39	0.935	4.315	4.809	1.205	0.690	1.273	894.5	10
^{40}S	30	0.990	2.571	7.926	1.207	0.690	1.272	1079	18

$\Delta\sigma_R$ is the relative difference between the total reaction cross section given by our folding analysis and that given by the mass- and energy dependent systematics for stable isotopes [48].

nucleus are 3.44 fm (3.24 fm), as reported in Table 2 of Ref. [21].

In an OM study of the elastic scattering induced by a neutron-rich nucleus, the isospin dependence of the optical potential should become more significant. While this effect is negligible in $^{30,32}\text{S}+p$ cases, it becomes more and more sizable in $^{36,38,40}\text{S}+p$ cases. From the prediction of the HF+BCS calculation for the neutron rich $^{36,38,40}\text{S}$ isotopes (see, e.g., Fig. 10 in Ref. [21]), the extra neutrons do not form the halo-like structure and they distribute evenly both in the interior and at the surface. As a result, the ground state neutron density is larger than the proton density at all radii. This difference determines the isovector part of the optical potential $V_0^{IV}(E, R)$, i.e., the microscopic estimation of the Lane potential [49]. Our results show that the maximal difference in the elastic scattering cross section, caused by the isovector potential $V_0^{IV}(E, R)$, is ranging from about 15% in $^{36}\text{S}+p$ case up to about 30% in $^{40}\text{S}+p$ case (see upper parts of Figs. 3 and 4). Although the difference found is still within the experimental errors of the measured elastic cross section, this result indicates that the isovector component of the proton-nucleus optical potential might be probed in accurate measurements of the elastic scattering induced by neutron rich beams. Such experiments could be an alternative study to (p,n) charge exchange reaction (where the isovector component of the nucleon-nucleus optical potential can be separately tested [50,51]).

4.2. Inelastic scattering

The present folding analysis of inelastic scattering data has been performed within the standard DWBA using the transition form factors defined in Eqs. (38) and (39). Since the effective NN interaction has been fine-tuned in the HF studies of symmetric [15] and asymmetric [18] nuclear matter, it is expected to be a quite reliable input for the folding calculation and the test of the QRPA transition densities in the folding + DWBA analysis. One can see in Table 2 that the proton parts of the QRPA transition densities for the lowest 2^+ states in $^{30,32}\text{S}$ give $B(E2)$ values very close to the experimental ones. The corresponding neutron transition densities were found to have about the same radial

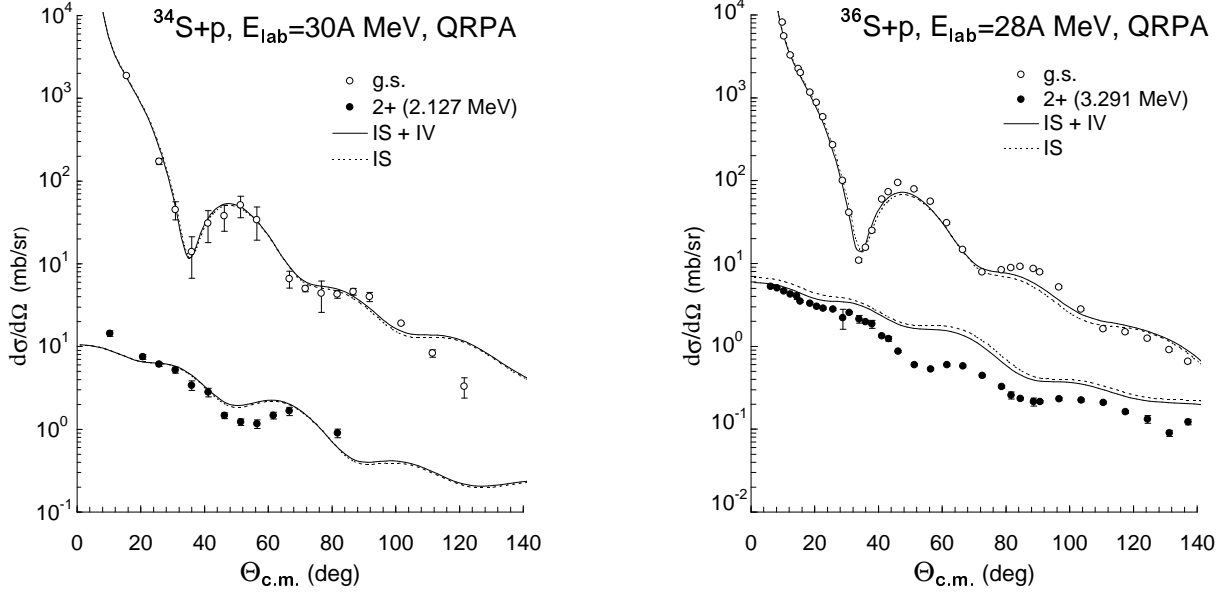


Figure 3. The same as Fig. 1 but for elastic and inelastic $^{34}\text{S}+\text{p}$ and $^{36}\text{S}+\text{p}$ data at $E/A = 30$ [22] and 28 MeV [23], respectively.

shape (see Fig. 11 in Ref. [21]) and they give, therefore, $M_{2+}^n/M_{2+}^p \approx N/Z$. From the DWBA results plotted in Fig. 1 one can see that the inelastic form factor calculated from the QRPA transition densities describes very well the inelastic $^{30,32}\text{S}+\text{p}$ scattering data measured recently at $E_{\text{lab}} = 53A$ MeV [21]. This confirms the microscopic structure of the lowest 2^+ states in $^{30,32}\text{S}$ predicted by the QRPA. Since the difference between the proton and neutron transition densities is very small for these two nuclei (especially for ^{32}S) the isovector component of the folded form factor is negligible and the DWBA cross section is determined mostly by the isoscalar form factor. In other words, the lowest quadrupole excitation in $^{30,32}\text{S}$ is predominantly isoscalar, with the best-fit moment ratio $M = (M_{2+}^n/M_{2+}^p)/(N/Z) \approx 1$.

We note that, given the accurate QRPA transition density (which has a proton part very close to the experimental charge transition density [21]) and well tested CDM3Y6 interaction [15], the new proton scattering data measured for the ($N = Z$) stable ^{32}S isotope turn out to be a very good test case for our folding approach. The fact that, without any scaling of the folded form factor, the DWBA cross section agrees perfectly with the inelastic $^{32}\text{S}+\text{p}$ data confirms the reliability of the present folding + DWBA approach in probing the structure of the lowest 2^+ states in Sulfur isotopes. This result also shows that the inelastic form factor folded with the CDM3Y6 interaction (which has been fine-tuned in the HF studies) can enter the DWBA calculation without a renormalization factor, i.e., $N_R = 1$ for the inelastic folded potential. As a result, the higher-order contribution from the DPP to the *real* inelastic form factor seems to be weaker than that to the real optical potential.

The DWBA folding results are compared with the $^{34,36}\text{S}+\text{p}$ scattering data in Fig. 3. With the predicted $B(E2)$ value about 20% larger than the experimental data for ^{34}S (see

Table 2), the agreement between the DWBA cross section with the inelastic data is still reasonably good for the $^{34}\text{S}+\text{p}$ system. In ^{36}S , the $B(E2)$ value given by the QRPA is roughly 2.5 times larger than the experimental one, and the DWBA cross section for the 2^+ excitation in ^{36}S consequently overestimates the data over the whole measured angular region, especially at large scattering angles. The damping of the lowest 2^+ excitation in ^{36}S , leading to a transition strength $B(E2)_{\text{exp}}$ about two times smaller than that observed for the lowest 2^+ states in neighboring Sulfur isotopes, cannot be explained within the current QRPA model. The neutron transition strength predicted by QRPA turns out to be quite weak and gives a moment ratio $M = (M_{2^+}^n/M_{2^+}^p)/(N/Z) \approx 0.64$. Several structure models together with the DWBA analysis of the same data using the form factor folded with the JLM effective interaction [21,25] have also failed to describe this nucleus. Thus, ^{36}S nucleus still remains a puzzle to theoreticians, and the structure models should start being able to reproduce its $B(E2)$ value. We will see below that some disagreement with the measured angular distribution remains after renormalizing the QRPA (proton)

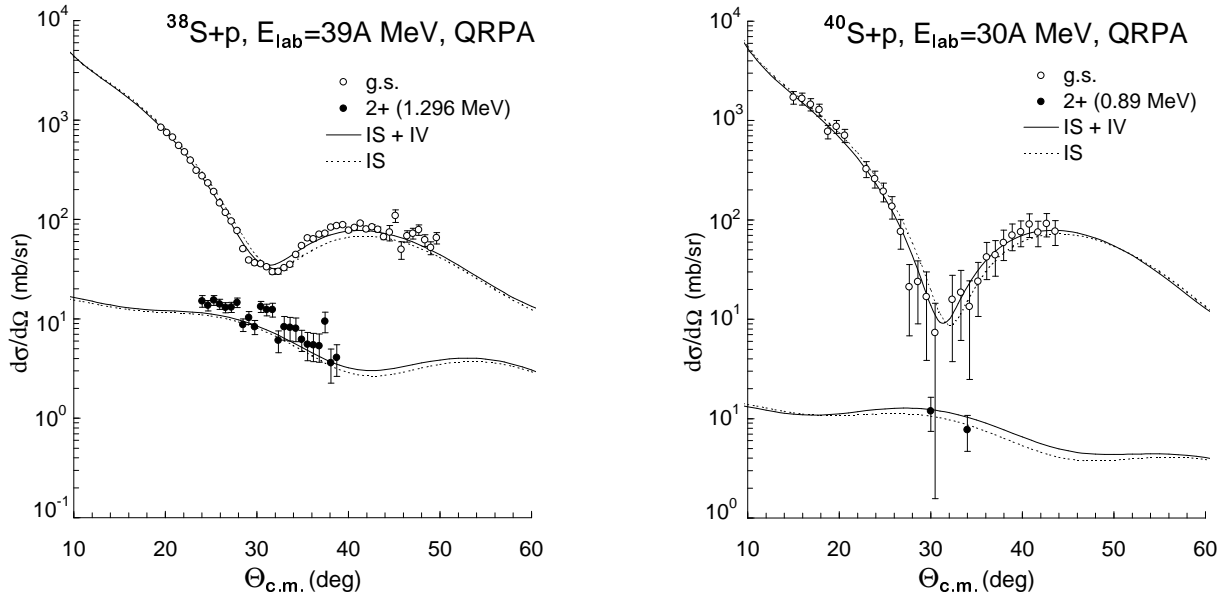


Figure 4. The same as Fig. 1 but for elastic and inelastic $^{38}\text{S}+\text{p}$ and $^{40}\text{S}+\text{p}$ data at $E/A = 39$ [24] and 30 MeV [25], respectively.

The DWBA results for $^{38,40}\text{S}+\text{p}$ systems are compared with the scattering data in Fig. 4. Even though the predicted $B(E2)$ value is about 40% larger than the experimental one in ^{38}S (see Table 2), the DWBA cross section underestimates the inelastic $^{38}\text{S}+\text{p}$ data by about 30%. This indicates that the QRPA neutron transition strength is somewhat weaker than that required by the inelastic data. The predicted moment ratio $M_{2^+}^n/M_{2^+}^p$ for ^{38}S is close to N/Z (the same as in ^{32}S) and it could also indicate a lack of neutron transition strength in the QRPA results. For ^{40}S , the predicted $B(E2)$ is about 30% larger than the experimental value and $M_{2^+}^n/M_{2^+}^p \simeq N/Z$ (see Table 2). However, it is difficult

to discuss about the proton and neutron transition strengths of the 2^+ state in ^{40}S based

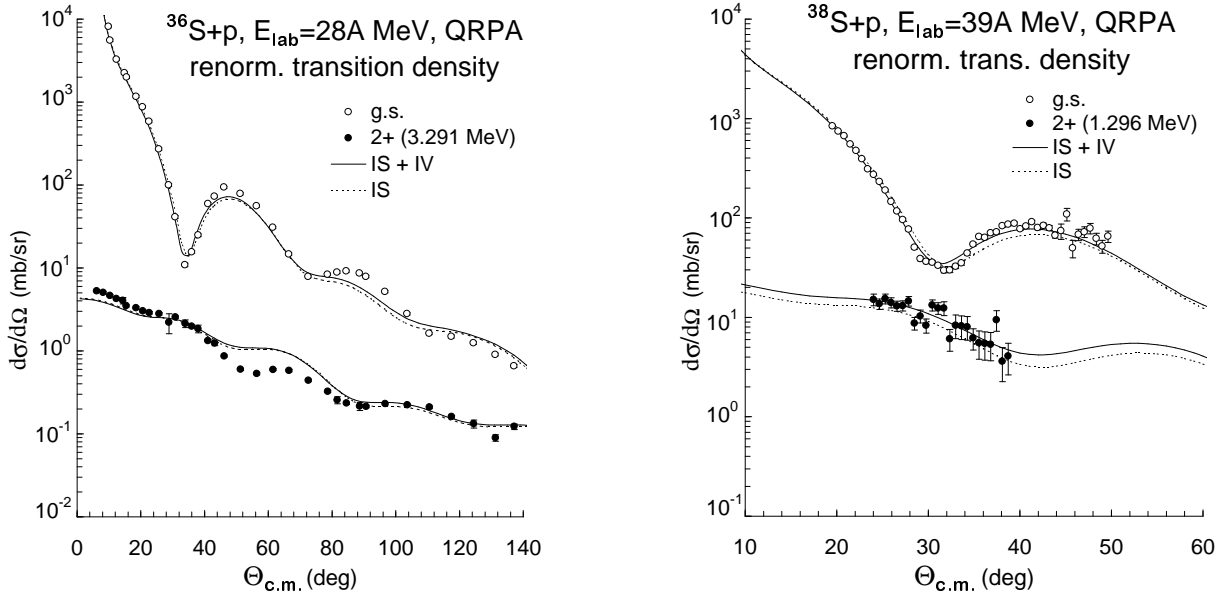


Figure 5. The same as Fig. 1 but for elastic and inelastic $^{36}\text{S}+p$ and $^{38}\text{S}+p$ data at $E/A = 28$ [23] and 39 MeV [24], respectively. Inelastic (transition) form factors folded with *renormalized* QRPA transition densities were used in the DWBA calculation (see details in Text).

Clearly, one can discuss quantitatively the transition strengths only when the theoretical model gives good description of both the $B(E2)_{\text{exp}}$ value and the measured inelastic angular distribution. For that purpose, we have further made the same folding + DWBA analysis of $^{34-40}\text{S}+p$ systems using an inelastic form factor obtained from *renormalized* QRPA transition densities, as done earlier by Khan *et al.* [21]. Namely, the proton part of the QRPA transition density is scaled to give the experimental $B(E2)_{\text{exp}}$ value and the neutron part is adjusted by the best DWBA fit to the inelastic scattering data. The moment ratio obtained in this way is denoted as M_{exp} in Table 2. Note that for $^{30,32}\text{S}$ isotopes, the QRPA transition densities give good description to both the $B(E2)_{\text{exp}}$ value and the measured inelastic scattering data, so that $M_{\text{exp}} = M_{\text{QRPA}}$. Among other cases, the improved agreement between the DWBA cross section and the data is clearly seen in Fig. 5 for the $^{36,38}\text{S}+p$ systems. One can notice that, even after the QRPA transition density is renormalized, there remains some disagreement with the inelastic $^{36}\text{S}+p$ data at medium angles. The scattering at medium and large angles is known to probe the form factor at sub-surface distance, and this effect might indicate a deficiency in the radial shape of the QRPA transition density for ^{36}S which cannot be changed by the renormalization procedure. The damping of the 2^+ excitation in ^{36}S can be judged by the scaling factors of the QRPA transition density: after the proton transition density is scaled down by a factor of 0.63 to give $B(E2) = B(E2)_{\text{exp}} \approx 96 e^2\text{fm}^4$, the neutron transition density needs to be renormalized by a factor of 0.88 to fit the inelastic data. Although the obtained

moment ratio ($M_{\text{exp}} \approx 0.90$) is larger than that predicted by QRPA for ^{36}S , it still shows

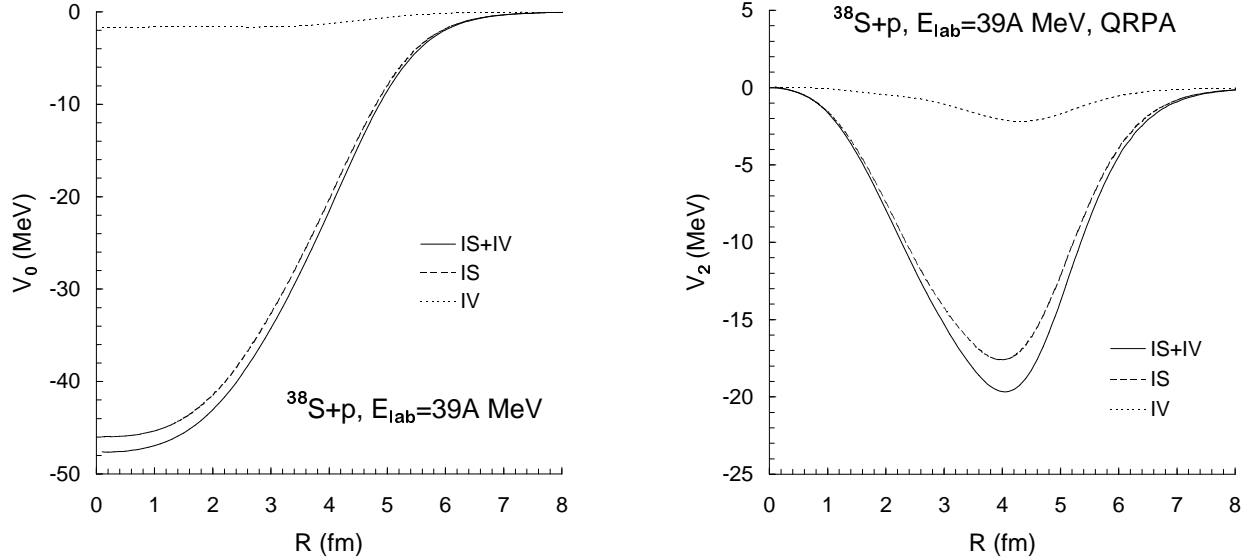


Figure 6. $^{38}\text{S}+\text{p}$ (real) optical potential (left panel) and inelastic form factor for the 2^+ excitation (right panel) folded with the HF+BCS ground-state and *renormalized* QRPA transition densities. Isoscalar and isovector components of the potentials are plotted as dashed and dotted curves, respectively.

The results obtained for the $^{38}\text{S}+\text{p}$ system are quite interesting. After the proton transition density was scaled by a factor of 0.85 to give the experimental $B(E2)_{\text{exp}}$ value, the neutron transition density needed to be renormalized by a factor of 1.25 for the best agreement of DWBA cross section with the inelastic data. As a result, the difference between the proton and neutron transition densities becomes larger and enhances the isovector contribution to the DWBA cross section. The 2^+ cross section given by the isovector part of the $^{38}\text{S}+\text{p}$ form factor is about 25-30% of the total 2^+ cross section. Such a significant contribution is due to a strong neutron transition strength ($M_{2^+}^n$) compared with the proton one ($M_{2^+}^p$) which gives the ratio $M_{\text{exp}} = 1.44$. The isovector mixing is slightly weaker in the elastic channel, with the cross section given by the isovector part of the $^{38}\text{S}+\text{p}$ optical potential of about 20% of the total elastic cross section. In Fig. 6, one can see that the difference ($\rho_p - \rho_n$) between the proton and neutron transition densities leads to an enhancement of the isovector part of the folded 2^+ form factor [see also Eqs. (26) and (30)] at distances around $R = 4$ fm, where $V_{2^+}^{IV}$ amounts up to 15% of the total form factor strength. Since the inelastic cross section is directly proportional to the square of the form factor, the 2^+ cross section given by the isovector part of the folded form factor alone (see Fig. 5) becomes around 25-30% of the total 2^+ cross section. For the elastic scattering the difference ($\rho_p - \rho_n$) between the proton and neutron ground-state densities is smaller, and the isovector part of the folded optical potential or the Lane

potential is about 7-9% of the total potential strength at radii near $R = 4$ fm (see left panel of Fig. 6), which leads to an isovector mixing of about 20% in the elastic $^{38}\text{S}+\text{p}$ cross section.

For $^{40}\text{S}+\text{p}$ system, the isovector mixing becomes stronger in the elastic channel, with the cross section given by the isovector part of the $^{40}\text{S}+\text{p}$ folded optical potential of about 30% of the total elastic cross section. However, the situation in the 2^+ inelastic channel is still uncertain because the best-fit ratio $M_{\text{exp}} = 1.17$ is based on two data points only. One clearly needs more experimental information in order to have a reliable estimate for the transition moment ratio in ^{40}S .

The comparison of the results using the same structure input but with two different reaction models (JLM approach and the present folding model) is of special interest, because of the extensive (p,p') data available along the Sulfur isotopic chain, including elastic and inelastic angular distributions. Although the JLM approach gives, in general, good agreement with the data, it appears to have some difficulties to reproduce both the first minimum and the elastic distribution at large angles (see Figs. 13, 14, 15 of Ref. [21], Fig. 9 of Ref. [25] and Fig. 7 of Ref. [52]). It is interesting to note that this feature does not happen with the present folding calculations. For the considered 2^+ excitations, the DWBA cross sections given by the inelastic form factors folded with the JLM interaction seem to overestimate the inelastic data in most cases which results in the smaller transition moment ratios compared to our study. First, one should note the radically different approaches of these two models. In the JLM approach, one uses the local density approximation (LDA) to obtain the local optical potential from that calculated for *infinite* nuclear matter, while in the folding model both the optical potential and inelastic form factor are calculated in the Hartree-Fock manner (with antisymmetrization treated properly) using a fine-tuned density dependent CDM3Y6 interaction that is based on the G-matrix elements of the Paris NN potential for *finite* nuclei. Therefore, the mentioned problem might well be due to the validity of the LDA and suggests further investigations to improve the JLM parameters. Another clue is that a better description of elastic data by the folding potential might also be due to the fact that the imaginary optical potential is based on CH89 global systematics [39], with its strength slightly adjusted to fit the elastic data. In this sense, the imaginary WS (elastic and transition) potentials obtained in our approach could serve as a good reference to improve the microscopic description of the imaginary part of the optical potential and the transition form factor for the considered cases. As discussed above, the ^{36}S case remains a common problem for both reaction models and the deficiency should be due to the structure model. Finally we note that the best-fit transition moment ratios deduced from our folding + DWBA analysis turned out to be quite close to those deduced earlier (see M_{exp} and M_{Phenom} values in Table 2) from the DWBA analysis of essentially the same data [21,25] using standard collective model form factor. This is very satisfactory in the sense that the microscopic analysis of the properties of stable and exotic nuclei, which is the final goal of this kind of approach, is independent from the reaction model, provided this reaction model is accurate enough.

5. CONCLUSION

A consistent single folding formalism for the proton-nucleus optical potential and inelastic form factor, using a realistic density dependent CDM3Y6 interaction based on the G-matrix elements of the Paris NN potential and the microscopic ground-state and transition densities given by the HF+BCS and QRPA calculations, respectively, has been applied to study elastic and inelastic scattering of $^{30-40}\text{S}$ isotopes on proton target. The contribution of the isovector part of the folded optical potential and inelastic form factor to the calculated elastic and inelastic cross section has been considered explicitly in all cases.

For the proton rich ^{32}S nucleus, the results of the OM and DWBA analyses reproduce very well the measured elastic and inelastic scattering data and do not indicate the existence of a proton halo in this nucleus. Our results have shown quite a strong isovector mixing in the elastic and inelastic $^{38,40}\text{S}+p$ scattering. In particular, the best fit strength of the isovector part of the form factor in the inelastic 2^+ channel for ^{38}S is significantly stronger than that predicted by the QRPA. The detailed folding + DWBA analysis of the considered data has closely reproduced the systematics found earlier (based on standard collective model form factors) [21,25] for the neutron-proton ratio of the 2^+ transition moments in neutron rich Sulfur isotopes.

In conclusion, the present folding + DWBA approach has been proven to be accurate and reliable in extracting the neutron and proton transition strengths $M_\lambda^{n(p)}$ of the nuclear excitation induced by the inelastic proton scattering. Moreover, our approach is very efficient in testing the microscopic nuclear densities and determining the isospin character of the considered excitation (in structure of the excited state as well as in the inelastic angular distribution).

These results confirm again that proton scattering induced by the neutron rich beams remains a very effective tool in nuclear structure study. Such measurements would allow us not only to test the ingredients of the microscopic structure models (like QRPA) but also the isospin dependence of the proton-nucleus optical potential and inelastic form factor (prototypes of the Lane potential) and, consequently, the isospin dependence of the in-medium NN interaction (which is a key to specify the equation of state for asymmetric nuclear matter [18]).

ACKNOWLEDGEMENTS

The present research was supported, in part, by Natural Science Council of Vietnam and Vietnam Atomic Energy Commission (VAEC).

REFERENCES

1. B. Sinha, Phys. Rep. 20 (1975) 1.
2. F.A. Brieva and J.R. Rook, Nucl. Phys. A 291 (1977) 299; Nucl. Phys. A 291 (1977) 317.
3. F.A. Brieva and J.R. Rook, Nucl. Phys. A 297 (1978) 206.
4. L. Rikus, K. Nakano and H.V. von Geramb, Nucl. Phys. A 414 (1984) 413.
5. P.J. Dortmans, K. Amos, S. Karataglidis and J. Raynal, Phys. Rev. C 58 (1998) 2249;

- K. Amos, P.J. Dortmans, S. Karataglidis, H.V. von Geramb and J. Raynal, Adv. in Nucl. Phys. 25 (2001) 275.
6. R.S. Mackintosh, Nucl. Phys. A 307 (1978) 365; B.Z. Georgiev and R.S. Mackintosh, Nucl. Phys. A 307 (1978) 377.
 7. T. Cheon, K. Takayanagi and K. Yazaki, Nucl. Phys. A 427 (1985) 301; Nucl. Phys. A 445 (1985) 227.
 8. H. Feshbach, Theoretical Nuclear Physics, Vol. II (Wiley, NY, 1992).
 9. G. Bertsch, J. Borysowicz, H. McManus and W.G. Love, Nucl. Phys. A 284 (1977) 399.
 10. N. Anantaraman, H. Toki and G.F. Bertsch, Nucl. Phys. A 398 (1983) 269.
 11. G.R. Satchler and W.G. Love, Phys. Rep. 55 (1979) 183.
 12. Dao T. Khoa and W. von Oertzen, Phys. Lett. B 304 (1993) 8.
 13. Dao T. Khoa and W. von Oertzen, Phys. Lett. B 342 (1995) 6.
 14. Dao T. Khoa, W. von Oertzen, H.G. Bohlen, G. Bartnitzky, H. Clement, Y. Sugiyama, B. Gebauer, A.N. Ostrowski, Th. Wilpert, M. Wilpert and C. Langner, Phys. Rev. Lett. 74 (1995) 34.
 15. Dao T. Khoa, G.R. Satchler and W. von Oertzen, Phys. Rev. C 56 (1997) 954.
 16. H.A. Bethe, Ann. Rev. Nucl. Sci. 21 (1971) 93.
 17. N. Van Giai, P.F. Bortignon, G. Colò, Z. Ma and M.R. Quaglia, Nucl. Phys. A 687 (2001) 44c.
 18. Dao T. Khoa, W. von Oertzen and A. A. Ogloblin, Nucl. Phys. A 602 (1996) 98.
 19. Dao T. Khoa and G.R. Satchler, Nucl. Phys. A 668 (2000) 3.
 20. E. Khan and Nguyen Van Giai, Phys. Lett. B 472 (2000) 253.
 21. E. Khan *et al.*, Nucl. Phys. A 694 (2001) 103.
 22. R. Alarcon, J. Rapaport, R.T. Kovzes, W.H. Moore and B.A. Brown, Phys. Rev. C 31 (1985) 697.
 23. A. Hogenbirk, H.P. Blok, M.G.E. Brand, A.G.M. van Hees, J.F.A. van Hienen and F.A. Jansen, Nucl. Phys. A 516 (1990) 205.
 24. J.H. Kelley *et al.*, Phys. Rev. C 56 (1997) R1206.
 25. F. Maréchal *et al.*, Phys. Rev. C 60 (1999) 034615.
 26. X. Campi and A. Bouyssy, Phys. Lett. B 73 (1978) 263.
 27. P. Ring and P. Schuck, The nuclear many-body problem, Springer-Verlag, New York, 1980, p.542.
 28. Dao T. Khoa, Phys. Rev. C 63 (2001) 034007.
 29. G.R. Satchler, Direct Nuclear Reactions, Clarendon Press, Oxford, 1983.
 30. J.P. Jeukenne, A. Lejeune and C. Mahaux, Phys. Rev. C 16 (1977) 80.
 31. D.M. Brink and G.R. Satchler, Angular Momentum, Clarendon Press, Oxford, 1993.
 32. J.K. Hamilton and R.S. Mackintosh, J. Phys. G 3 (1977) L19 and J. Phys. G 4 (1978) 557.
 33. M. El-Azab Farid and G.R. Satchler, Nucl. Phys. A 481 (1988) 542.
 34. R.A. Broglia, C.H. Dasso, G. Pollarolo and A. Winther, Phys. Rep. 48 (1978) 351.
 35. D.A. Varshalovic, A.N. Moskalev and V.K. Khersonskii, Quantum Theory of Angular Momentum, World Scientific Publishing, 1988, p.167.
 36. W.G. Love, Nucl. Phys. A 192 (1972) 49.
 37. Dao T. Khoa, G.R. Satchler and W. von Oertzen, Phys. Rev. C 51 (1995) 2069 .

38. J. Raynal, Computing as a Language of Physics (IAEA, Vienna, 1972) p.75; J. Raynal, coupled-channel code ECIS97 (unpublished).
39. R.L. Varner, W.J. Thompson, T.L. McAbee, E.J. Ludwig and T.B. Clegg, Phys. Rep. 201 (1991) 57.
40. G. Colò and P.F. Bortignon, Nucl. Phys. A 696 (2001) 427.
41. S. Raman, C. H. Malarkey, W. T. Milner, C. W. Nestor, and P.H. Stelson, At. Data and Nucl. Data Tables 36 (1987) 1.
42. H. Scheit *et al.*, Phys. Rev. Lett. 77 (1996) 3967.
43. T. Glasmacher *et al.*, Phys. Lett. B 395 (1997) 163.
44. Nguyen Van Giai and H. Sagawa, Nucl. Phys. A 371 (1981) 1.
45. A. Bohr and B. Mottelson, Nuclear Structure, Benjamin, New York, 1969, Vol. 1, p. 169.
46. A.M. Bernstein, V.R. Brown and V.A. Madsen, Comm. Nucl. Part. Phys. 11 (1983) 203.
47. A. Ozawa, T. Suzuki and I. Tanihata, Nucl. Phys. A 693 (2001) 32.
48. R.F. Carlson, At. Data and Nucl. Data Tables 63 (1996) 93.
49. A.M. Lane, Phys. Rev. Lett. 8 (1962) 171.
50. M.D. Cortina-Gil *et al.*, Nucl. Phys. A 641 (1998) 263.
51. A. de Vismes *et al.*, Phys. Lett. B 505 (2001) 15; A. Pakou *et al.*, Nucl. Phys. A 691 (2001) 661.
52. H. Scheit *et al.*, Phys. Rew. C 63 (2000) 014604.